

MIT Open Access Articles

Toward automated detection of malignant melanoma

The MIT Faculty has made this article openly available. **Please share** how this access benefits you. Your story matters.

Citation: Huang, Billy, and Daniel S. Gareau. "Toward automated detection of malignant melanoma." Advanced Biomedical and Clinical Diagnostic Systems VII. Ed. Anita Mahadevan-Jansen, Tuan Vo-Dinh, & Warren S. Grundfest. San Jose, CA, USA: SPIE, 2009. 71690X-9. © 2009 SPIE

As Published: <http://dx.doi.org/10.1117/12.809386>

Publisher: Society of Photo-optical Instrumentation Engineers

Persistent URL: <http://hdl.handle.net/1721.1/54722>

Version: Final published version: final published article, as it appeared in a journal, conference proceedings, or other formally published context

Terms of Use: Article is made available in accordance with the publisher's policy and may be subject to US copyright law. Please refer to the publisher's site for terms of use.



Toward automated detection of malignant melanoma

Billy Huang^{1,2}, Daniel S. Gareau^{1,3}

1. Memorial Sloan-Kettering Cancer Center New York, NY

2. Currently at Massachusetts Institute of Technology
Cambridge, MA

3. Currently at Oregon Health & Science University
Portland, OR

Abstract: In vivo reflectance confocal microscopy shows promise for the early detection of malignant melanoma (MM). Two hallmarks of MM have been identified: the presence of pagetoid melanocytes in the epidermis and the breakdown of the dermal papillae. For detection of MM, these features must be identified qualitatively by the clinician and qualitatively through automated pattern recognition. A machine vision algorithm was developed for automated detection. The algorithm detected pagetoid melanocytes and breakdown of the dermal/epidermal junction in a pre-selected set of five MMs and five benign nevi for correct diagnosis.

Keywords: automated detection, confocal, melanoma

INTRODUCTION

Malignant Melanoma (MM) is the most fatal form of skin cancer, with an estimated mortality rate of 14%^[1]. The incidence of MM is increasing in the United States with an estimated 60,000 new cases last year alone in the US (an increase of over two percent from the previous year)^[1]. Because of the tendency for MM's to metastasize, early detection and excision are critical. Melanomas are thought to originate in the dermal-epidermal junction (DEJ) and progress in lateral and vertical growth phase leading to metastasis.

The current methods of removing MM's include standard surgical excisions, chemotherapy, radiation therapy, and immunotherapy, each with varying success. The five-year survival rates for melanoma is approximately 90%, with percentages ranging from 100% (stage 0 removal) to less than 17% (stage 4)^[2].

This work aims to exploit the optical sectioning capability of reflectance-mode confocal scanning laser microscopy (CSLM) to non-invasively survey the DEJ, noting the irregularities associated with malignancy. Comprehensive diagnosis and subsequent treatment of melanoma have so far required both reliable imaging technologies and the trained eye of a clinician for assessment.

The objective of this study was to create an algorithm to assist the clinician in diagnosing MM, specifically through computer vision of skin lesions. CSLM is a proven imaging modality, with the capability to offer axial resolution of 3- μm ^[3] and fields-of-view up to centimeters^[4]. Due to the backscattering nature of melanin ($\eta = 1.72$) in epidermis ($\eta = 1.34$), confocal imaging proves applicable in detecting subsurface melanocytes. Melanin is highly backscattering, and as such, provides good contrast for confocal imaging^[5] and heavily melanotic lesions appear with bright contrast. The limitations of imaging skin via confocal microscopy *in vivo* include the non-uniform density of the medium as well as the lack of penetration permitted by typical excitation wavelengths. With near-infrared excitation, a penetration depth of 350 μm can be achieved; sufficient for penetration and imaging of the superficial reticular dermis^[6]. Recent studies by Langley et al. (2001), Tannous et al. (2002), Gerger et al. (2004), and Gareau et al. (2007) have demonstrated the feasibility of *in vivo* confocal imaging through melanocytic lesions in both human and murine

models^[7-10].

The most prevalent histological hallmark of melanoma is the presence of pagetoid melanocytes above the basal layer which sometimes form irregularly sized nests. Pagetoid melanocytes or “pagetoid spread”, pertaining to the lateral growth phase, are detectable in both conventional histopathology and confocal imaging. Since pagetoid melanocytes in suspicious lesions typically reside above the basal layer (i.e. $<50\ \mu\text{m}$ beneath the stratum corneum), they are easily penetrated by confocal wavelengths and imaged.

Our melanoma processing algorithm is derived from processing a 3D confocal (z) volume of images taken by a clinician of a suspicious lesion and deducing the z location of the first reflective surface (FRS) at each x-y position, where we believe the most superficial melanin resides. The FRS (the layer of images which exhibited greater reflectance than its adjacent layers in a confocal volume) was hypothesized to be either the DEJ for benign skin or the locations of the pagetoid melanocytes, which are generally above the DEJ. Thus by creating 3D surface plot of the FRS for each point, it is possible to identify atypical structures or cells based on the relative depth of their FRS.

The second objective of the study was to represent the surface plot in two dimensions (i.e. an overhead z-view), and create a masking algorithm to systematically highlight shapes such as circles and ellipses which resembled cells. The composition of the surface compilation algorithm and the masking algorithm directly processes the raw confocal volume into a 2D image which highlights suspected cellular structures such as pagetoid melanocytes at a high reflective surface.

MATERIALS & METHODS

Confocal Stacks

3D, *in vivo* confocal image-cubes were obtained through the Dermatology Service at Memorial Sloan-Kettering Cancer Center (New York, NY). Images were identified with study protocol numbers and patient care was completely unaffected. Ten patients, each with multiple lesions, were imaged *in vivo* and *en face* with a commercially available VivaScope 1500™ (Lucid Inc., New York) without any exogenous dyes. Point illumination was provided by a near infrared laser at 850 nm. A custom 30X water immersion objective lens with a numerical aperture of 0.9, coupled to the patient through a glass window with gel ($n=1.34$), provided a $500\ \mu\text{m}$ field-of-view. The optical sectioning (axial resolution) was $<3\ \mu\text{m}$ and the lateral resolution was $<1\ \mu\text{m}$. Stacks were acquired in reflectance mode from lesions in the chest, scalp, thigh, and cheek. Each stack composed of 60 layered images, with the distance between each successive z-layer being $1\ \mu\text{m}$ deeper.

Machine Vision Algorithm

The image processing algorithm was created using MATLAB 7.4™ (Mathworks) coding and consists of several sub-algorithms, each which completed specific tasks. Raw confocal data was rearranged into a contiguous volume-cube matrix. Due to natural patient movement during imaging, the z-slices of confocal data are generally not aligned (x-y-shift between each layer). As such, an iterative guessing algorithm was developed to eliminate distortions caused by movement. The guessing algorithm shifts two successive images laterally until their error is minimized. The process is repeated for all the images in the stack and a new cube matrix is created and saved as a .mat file.

A second algorithm divided the volume into $700\times 700\times 60$ equidistant point-volumes on the x-

y plane and found the FRS for each of those point-volumes. The main assumption that the algorithm employed was that the FRS of the skin was either a pagetoid melanocyte or the dermal-epidermal junction. For each point, the algorithm ran through the axial intensity profile $R(Z)$ which was $60\text{ }\mu\text{m}$ deep with increments of $1\text{ }\mu\text{m}$ per layer, and identified the layer (FRS) the brightest pixel on the background corrected axial profile. Figure 1 illustrates this technique.

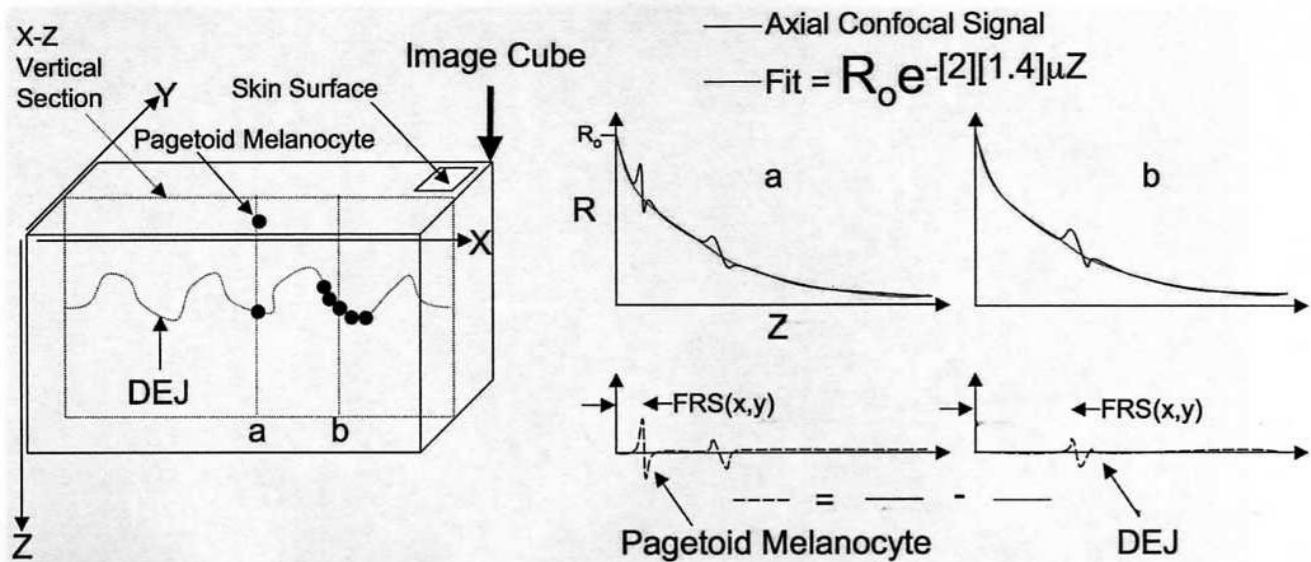


Figure 1. Confocal reflectance as a function of z-depth at (a) the location of a pagetoid melanocyte and (b) at a benign location. The signal (R , black line) is corrected for background reflectance by subtracting the fit to the data (red line) which chose R_0 and μ to minimize the least squares error. The first reflective surface (FRS) is determined as the maximum of the background-corrected data.

Since the penetrative power of the laser decays exponentially with imaging depth, it can be modeled with an inverse exponential (e) function. We used a exponential function to fit for the brightness of most superficial point-volume and axial decay rate. The predicted function assumes that there are no irregularities, such as the FRS, in the exponential axial decay. A background-correction was employed by subtracting the predicted function from the actual results, resulting in a straight light except for the location of the FRS where background correction curve exhibits a peak. The current limitation in this is number of points analyzed, which is limited by computing power.

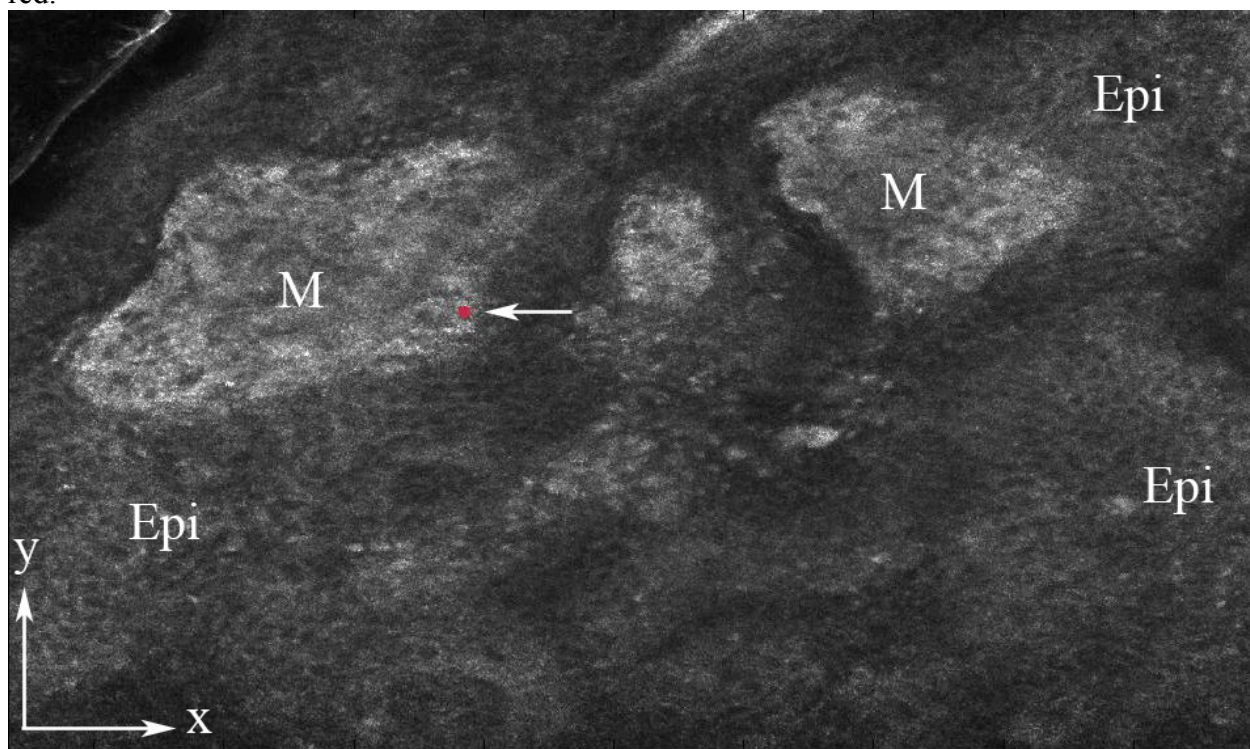
A third algorithm, the masking algorithm, created a mask of a certain size and shape given a numerical function. A simple function used was an ellipse, which approximates the shape of pagetoid cells. By multiplying the original mask by a constant (the average pixel intensity of the composite surface plot), the modified mask is able to accurately represent the cellular shapes and intensities of the surface plot. The masking algorithm applies the mask across the surface plot and produces an error estimate (difference) relating the accuracy of the mask. A thresholding code eliminated correlations below a specified level thereby highlighting regions with high reflective surfaces and identifies pagetoid melanocytes. A second image of the error estimate is produced; if the error is low, the location will appear bright, and high errors appear dark. The second image highlighted locations in which the mask-to-plot error is low, thus identifying locations where pagetoid melanocytes might

be located. For instance, a cell would appear bright because the error or difference between the mask and itself is low, while collagen fibers would appear less bright because the error between the mask and the collagen fibers (which are not shaped like the mask) is high.

RESULTS

The combination of the surface plot of the FRS and the masking algorithms detected the depth of brightest reflectance and highlighted these locations of interest, making it unequivocally simpler to identify possible pagetoid melanocytes.

Once the algorithm fit the axial data for a particular z location of the FRS (illustrated in figure 1), the entire lateral data set (x - y optical section) was extracted from the image cube for verification. Figure 2 shows the x - y section for the FRS z , value found at the x - y point marked in red.



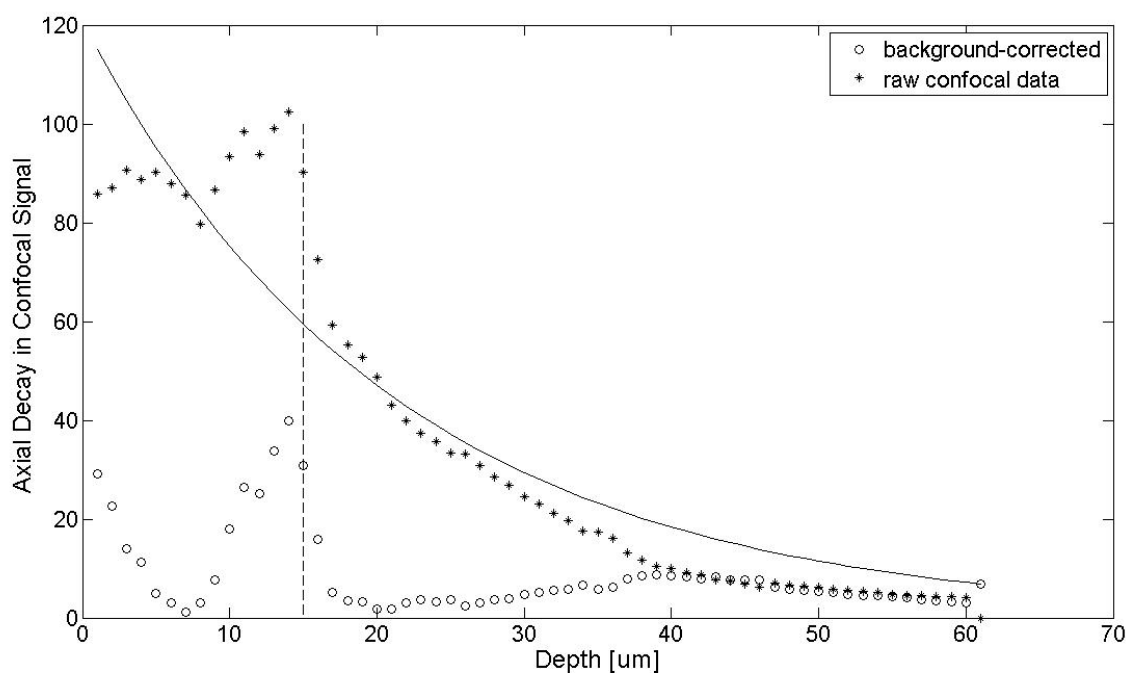


Figure 2. A confocal reflectance optical section (A) shows the epidermis (Epi) with the presence of melanocytic nests (M). The red dot (arrow) shows the location that yielded the z value as the FRS that identified this image. The dot is on the “ledge” of a vertical protrusion of melanocytic invasion of the epidermis. An axial decay is shown both before and after background correction (B). The first reflective surface is defined as the peak of the corrected data.

A surface plot of the depth at which the brightest pixel is located was compiled from the analysis of each point, thus creating a contour map of the FRS for each and every point. The higher the FRS is for a given point, the higher it was represented in the surface plot. By taking the average of 700x700x60 (x,y,z) points for each volume, a fairly accurate surface plot of the entire sample can be compiled. An analogy for the surface plot of the FRS is a cross-sectional view of rolling hills with telephone poles. The varying heights of the hills represent the varying depths of the DEJ while each telephone pole represent a column that rises out of the hills, namely each pagetoid melanocytes.

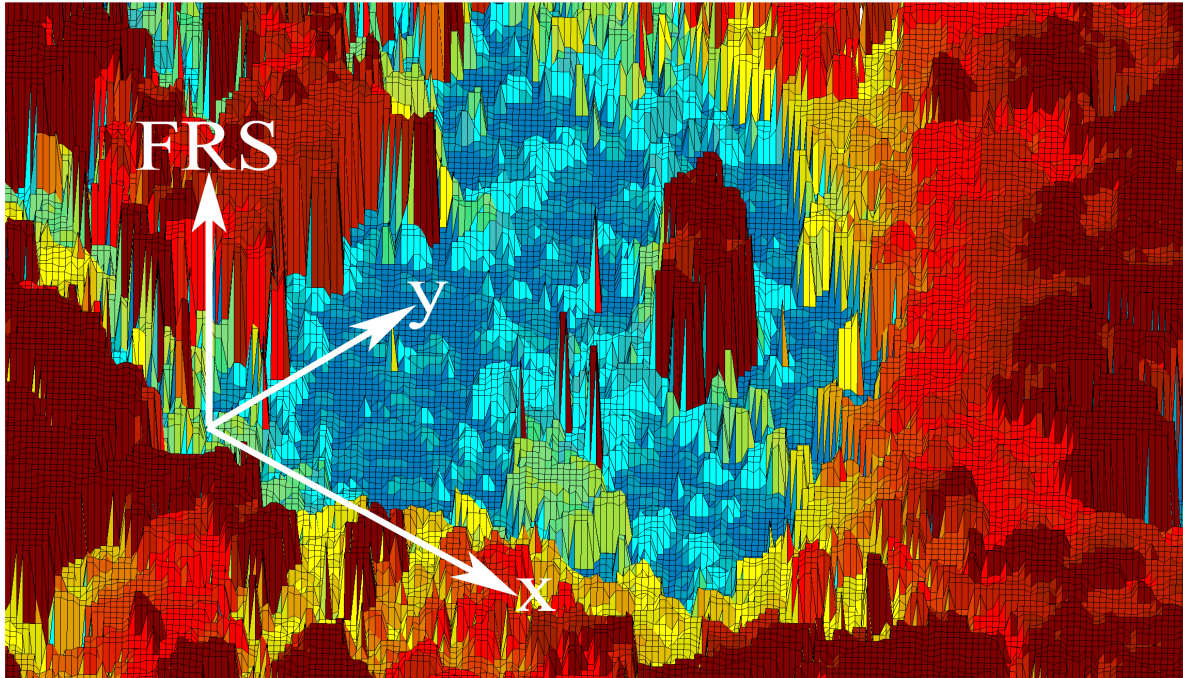


Figure 3. A 3D reconstruction of the FRS. The regions on the left and right of the image are the hills of the putative DEJ. In the center trough (blue) a single pagetoid melanocyte (red) is seen to rise above the DEJ.

Masking algorithm

The surface plot created a gradient scale of the first reflective surface. In cases where the FRS was not broken severely by a pagetoid melanocyte, the masking algorithm produced images where the intensity in two dimensions (x-y) revealed the cellular morphology at the dermal epidermal junction regardless of the epidermis or stratum corneum. Figure 4 a,b shows a case of lentigo maligna under such conditions.

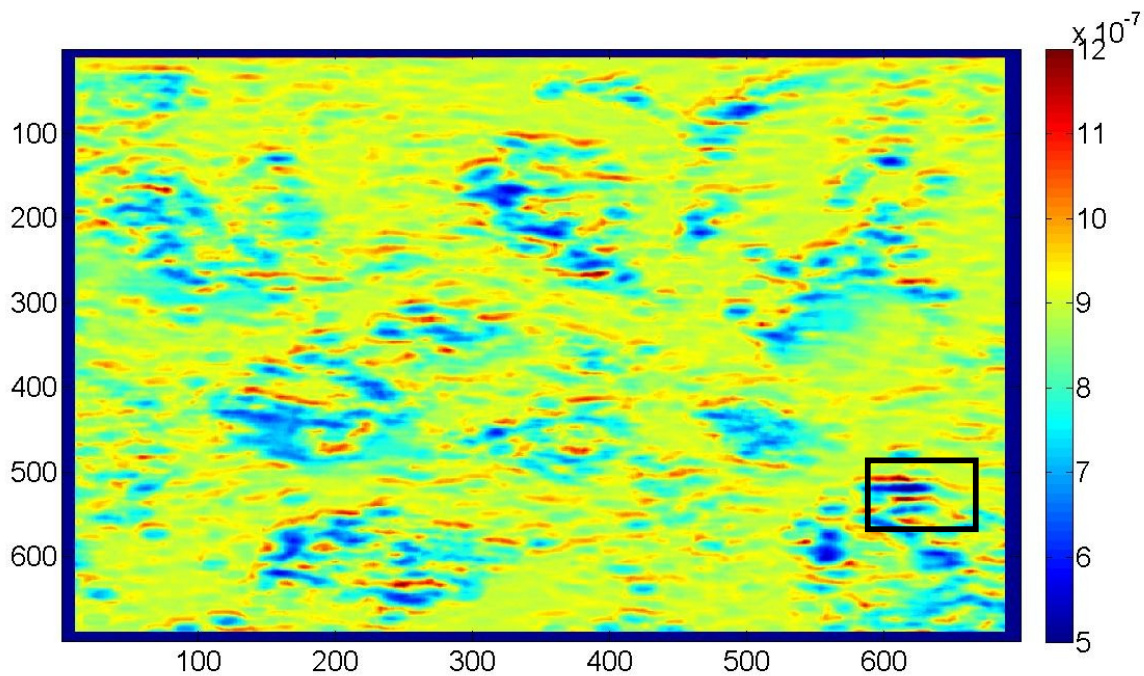


Figure 4a. The masked FRS for lentigo maligna shows the cellular architecture at the DEJ. The inset shows a region of highly reflective cells.

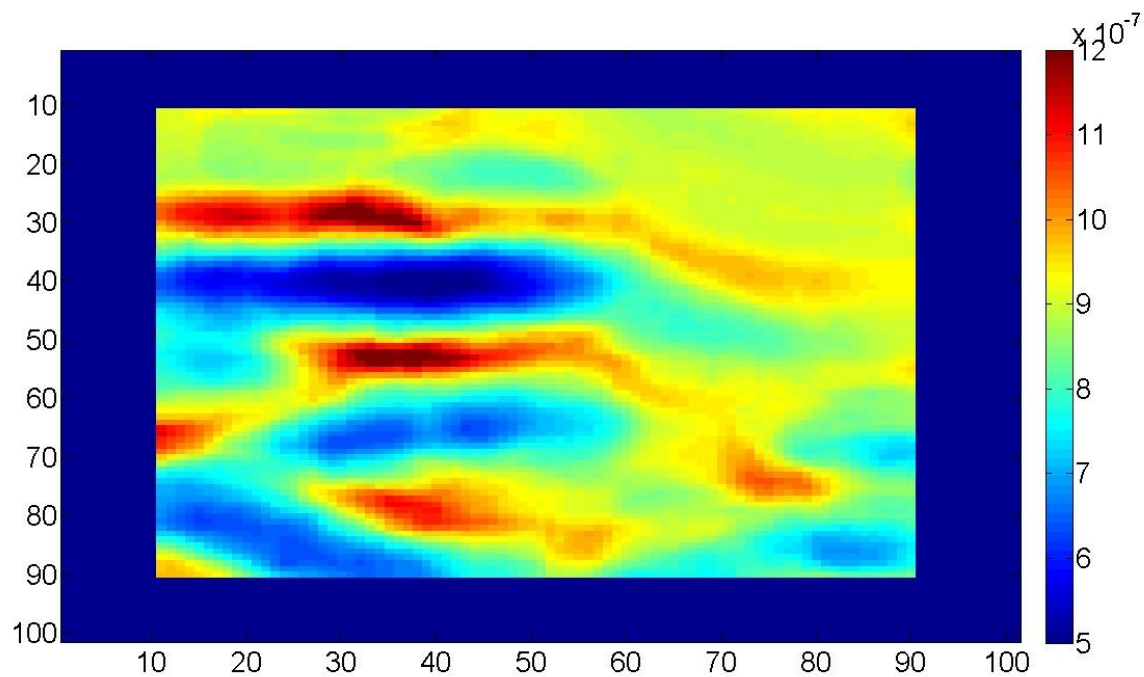


Figure 4b. An inset of the above masked surface (Fig. 4a) shows cells. The highly valued red regions to in the left-center shows the identification of the pagetoid melanocyte. In this region, the shape of

the cell, matched the shape of the mask well and the strong correlation enabled identification.

DISCUSSION

A feasible algorithm to facilitate the detection, of malignant melanoma will be of use to the clinician. The current method of detecting and diagnosing MM's include the ABCD (asymmetry, border, color, and diameter) method, followed by standard biopsies. New methods of detecting MM's, such as confocal microscopy, now offer an alternative non-invasive approach to detecting melanoma.

In this study, lesions which contain suspected pagetoid melanocytes were imaged using a confocal microscope *in vivo*, and the corresponding stack of images were analyzed using the machine vision algorithm. Because a cell is located in a 3D plane within the skin, going through a confocal stack to identify suspicious cells can be tedious. The object of the algorithm is to precisely locate suspect cells, and to aid in confirming the clinician's diagnosis. In our study, the algorithm correctly identified several cells, which correlated to the confocal image. Selected skin lesions were identified as dysplastic nevi through biopsies, some exhibiting the presence of pagetoid melanocytes. In order to further clarify the potential power of an automated detection algorithm, other hallmarks of malignant melanoma must be examined as well as examining a set of unequivocally malignant lesions. Other malignant features include the breakdown of the dermal-epidermal junction, cytological atypia, and irregular and confluent nests of melanocytes¹¹.

Further steps must be taken in order for this algorithm to describe the presence of melanoma accurately. Firstly, as mentioned previously, other features of melanoma must be taken into account in order for the clinician to make a clear diagnosis. Secondly, artifacts in the imaging must be taken into account since unusually bright or dark pixels tend to limit the accuracy of the both the raw data as well as the predicted function. Thirdly, a better mask can be made to describe the size and shapes of the cells in the stacks. The mask used in this study was an ellipse, although in many cases the morphology of atypical cells vary. In sum, the description of each of these factors varies from patient to patient, and the more information that can be processed, the more accurate the diagnosis.

Automated detection of melanoma is a novel alternative to typical biopsies. The development in confocal microscopy has led to potentially non-invasive methods of diagnosing skin cancer. The automated identification of possible tumors offers a supplement to the clinician's eye and may prove useful in making a diagnosis.

References

1. Jemal A, Siegel R, Ward E, Murray T, Xu J, Thun MJ (2007). Cancer Statistics, 2007. *CA Cancer J Clin.* 57, 43-66.
2. Five Year Survival Rates. Retrieved December 2, 2008, from Seer's Training Web Site Web site: http://training.seer.cancer.gov/ss_module14_melanoma/unit01_sec05_survival_rates.html
3. Gareau DS, Patel YG, Li Y., Aranda I, Halpern AC, Nehal KS, Rajadhyaksha M (2008). Confocal mosaicing microscopy in skin excisions: a demonstration of rapid surgical pathology. *Journal of Microscopy*. (Received 18 January; Accepted 18 July 2008, in press).
4. Gareau D, Li Y, Huang B, Eastman Z, Nehal K, Rajadhyaksha M (2008). Confocal mosaicing microscopy in

Mohs skin excisions: feasibility of rapid surgical pathology. *Journal of Biomedical Optics*. 13, 054001.

5. Rajadhyaksha M, Grossman M, Esterowitz D, Webb R, Anderson R (1995). In Vivo Confocal Scanning Laser Microscopy of Human Skin: Melanin Provides Strong Contrast. *Journal of Investigative Dermatology*. 104, 946-952.
6. Rajadhyaksha M, Gonzalez S, Zavislan J, Anderson R, Webb R (1999). In Vivo Confocal Scanning Laser Microscopy of Human Skin II: Advances in Instrumentation and Comparison With Histology. *Journal of Investigative Dermatology*. 113, 293-303.
7. Langley R, Rajadhyaksha M, Dwyer P, Sober A, Flotte T, Anderson R (2001). Confocal scanning laser microscopy of benign and malignant melanocytic skin lesions in vivo. *Journal of the American Academy of Dermatology*. 45, 365-376.
8. Tannous Z, Mihm M, Flotte T, Gonzalez S (2002). In vivo examination of lentigo maligna and malignant melanoma in situ, lentigo maligna type by near-infrared reflectance confocal microscopy: Comparison with in vivo images with histologic sections. *Journal of the American Academy of Dermatology*. 46, 260-263.
9. Gerger A, Koller S, Kern T, Massone C, Steiger K, Richtig E et al. (2005). Diagnostic Applicability of in Vivo Confocal Laser Scanning Microscopy in Melanocytic Skin Tumors. *Journal of Investigative Dermatology*. 124, 493-498.
10. Gareau DS, Merlino G, Corless C, Kulesz-Martin M, Jacques SL (2007). Noninvasive Imaging of Melanoma with Reflectance Mode Confocal Scanning Laser Microscopy in a Murine Model. *Journal of Investigative Dermatology*. 127, 2184-2190.
11. Urso C, Rongioletti F, Innocenzi D, Batolo D, Chimenti S, Fanti P et al. (2005). Histological features used in the diagnosis of melanoma are frequently found in benign melanocytic naevi. *Journal of Clinical Pathology*. 2005, 409-412.